Correlations of the feedback energy and BCG radio luminosity in galaxy clusters

Asif Iqbal,[1]⋆ Ruta Kale,[2]⋆ Biman B. Nath[1] and Subhabrata Majumdar[3]

[1]*Astronomy & Astrophysics, Raman Research Institute, Sadashiva Nagar, Bangalore 560080, Karnataka, India*

[2]*National Centre for Radio Astrophysics, Tata Institute of Fundamental Research, Pune 411007, Maharashtra, India*

[3]*Department of the Theoretical Physics, Tata Institute of Fundamental Research, 1 Homi Bhabha Road, Mumbai 400005, Maharashtra, India*

ABSTRACT

We study the excess entropy and the corresponding non-gravitational feedback energy (E_{feedback}) in the intra-cluster medium (ICM) by considering a sample of 38 galaxy clusters using *Chandra* X-ray and NRAO VLA Sky Survey/Giant Metrewave Radio Telescope radio observations. We find moderate correlation of the feedback energy and brightest cluster galaxy (BCG) radio luminosity (L_R) with the various cluster thermal properties. We show conclusively that the active galactic nucleus is more effective in transferring feedback energy to the ICM in less massive clusters. We find that within $0.3r_{500}$, the feedback energy correlates with cluster temperature as $E_{\text{feedback}} \propto T_{\text{obs}}^{0.98\pm0.37}$. Moreover, for radio-detected BCG sample, we find that BCG radio luminosity at 1.4 GHz scales with gas mass as $L_R \propto m_{\text{g,obs}}^{1.76\pm0.71}$ and with an X-ray luminosity as $L_R \propto L_{\text{X,obs}}^{0.94\pm0.35}$. Finally, we discuss the implications of our results with regard to feedback in clusters.

Key words: galaxies: clusters: intra-cluster medium – cosmological parameters.

1 INTRODUCTION

Galaxy clusters that grow through mergers in hierarchical structure formation play an important role in astrophysics and cosmology (Gladders et al. 2007). The total mass of the galaxy clusters comprises main dark matter component ($\approx$85 per cent), hot intra-cluster medium (ICM; $\approx$10 per cent), and remaining in the form of stellar matter, all of which are studied directly/indirectly with the help of X-ray, optical, and gravitational lensing observations (Bartelmann & Schneider 2001; Pratt et al. 2010).

In galaxy clusters, a convenient way of describing the thermodynamical properties of the ICM is through the entropy which is usually defined as $K_g(r) = k_B T n_e(r)^{-2/3}$, where k_B is the Boltzmann constant, n_e is the electron number density, and T is the temperature of ICM. By knowing the entropy distribution and the total mass distribution, one can determine the density/temperature of the ICM using a hydrostatic equilibrium equation with a suitable boundary condition (Nath & Majumdar 2011).

Several observations have found higher gas entropy (Pratt et al. 2010; Eckert et al. 2013) than predicted by non-radiative hydrodynamical simulations (Voit, Kay & Bryan 2005), especially, near cluster centres. It has now become clear that various complex non-gravitational processes like feedback from active galactic nucleus (AGN), radiative cooling, and supernovae play a vital role in modifying the thermal structure of ICM (Nath & Roychowdhury 2002;

Roychowdhury, Ruszkowski & Nath 2005; Chaudhuri, Nath & Majumdar 2012; Iqbal et al. 2017a). Investigation of non-thermal phenomena from radio observations and simulations has revealed radio-mode AGN feedback based on bubble injection as a dominant role in adding feedback energy (McNamara & Nulsen 2007; Gaspari et al. 2014).

The excess entropy and the corresponding feedback energy can be estimated by comparing the observed thermodynamic quantities with that of the theoretical non-feedback (non-radiative) model (Chaudhuri et al. 2012; Iqbal et al. 2017a). In particular, Chaudhuri et al. (2012) and Chaudhuri, Majumdar & Nath (2013) using *XMM–Newton* data found mean energy per particle to be 2.74 ± 0.87 keV up to r_{500}. Similarly, Iqbal et al. (2017a,b) showed that feedback profiles become consistent with zero in the cluster outer regions ruling out pre-heating scenarios.

In this *letter*, we use a sample of 38 galaxy clusters having both *Chandra* X-ray data from the ACCEPT sample of Cavagnolo et al. (2009)[1] and NRAO VLA Sky Survey (NVSS)/Giant Metre-wave Radio Telescope (GMRT) radio data from Kale et al. (2015a) to quantify the correlations of the energy feedback and brightest cluster galaxy (BCG) radio luminosity with related cluster bulk properties. In particular, we show that AGN feedback is more efficient in less massive clusters. Unlike previous analysis of Chaudhuri et al. (2013), who used average radio fluxes of all the sources near the cluster centre, we use radio data from the optically identified BCGs

[1]https://web.pa.msu.edu/astro/MC2/accept/clusters/

to study the correlations. We adopt a cosmology with $H_0 = 70$ km s^{-1} Mpc^{-1}, $\Omega_M = 0.3$, and $\Omega_\Lambda = 0.7$.

2 CLUSTER-BCG SAMPLE

We started with the parent sample of BCGs identified in galaxy clusters in the Extended GMRT Radio Halo Survey (EGRHS; Kale et al. 2015a). The EGRHS sample consists of clusters in the redshift range 0.2–0.4 that have X-ray luminosities, $L_{X[0.1-2.4\,\mathrm{keV}]} > 5 \times 10^{44}$ erg s^{-1} and declinations $>-31°$ (Venturi et al. 2008; Kale et al. 2015b). Only those clusters from EGRHS that were present in the ACCEPT sample were selected for this study. This led to a final sample of 38 clusters[2] with their corresponding BCGs as shown in Table 1: 23 with confirmed radio detected BCGs and 15 with upper limits to the radio powers (radio non-detection BCGs). The 'cool-core' (CC) or 'non-cool-core' (NCC) classification of the dynamical state of the cluster as used in Kale et al. (2015b) is given in column 2 of Table 1. This classification is based on the X-ray morphological parameters, namely power ratio (P_3/P_0), centroid shift (w_{500}), and concentration (c_{100}), that are described in Cassano et al. (2010). They classify a cluster as NCC if $P_3/P_0 > 1.2 \times 10^{-7}$, $w_{500} > 0.012$, and $c_{100} < 0.20$. It is important to note that radio-detection sample is dominated by the CC clusters (17 out of 20) while as a non-detection sample is dominated by NCC clusters (12 out of 18). The 1.4 GHz radio powers of the BCGs from Kale et al. (2015a) included the K-correction. A spectral index[3] of 0.8 for the radio continuum spectra of the BCGs was assumed. For the BCGs that were not detected in radio bands, the upper limits at 1.4 GHz correspond to five times the rms noise (5×0.45 mJy beam^{-1}) in the NVSS (Condon et al. 1998).

3 NON-RADIATIVE MODEL OF ICM

The ICM is taken to sit in the gravitational potential of the dark matter halo having a Navarro–Frenk–White (NFW) density profile (Navarro, Frenk & W 1996) characterized by $\rho_{dm} = \frac{\rho_s}{x(1+x)^2}$, where $x = r/r_s$, r_s is the scale radius and ρ_s is the normalization factor in units of density. The concentration parameter is given by $c_\Delta = r_\Delta/r_s$, where Δ is defined such that r_Δ is the radius out to which mean matter density is $\Delta\rho_c(z)$, $\rho_c(z)$ being critical density of the Universe at redshift z. We use m_{500} from Planck Collaboration XXIX (2013)[4] with the exception of clusters RX J1532.9+3021 (MACS J1532.8+3021), ZwCl 0857.9+2107 (ZWICKY 2089), and ZWICKY 2701 whose values were taken from Mantz et al. (2010). Further, we fix the NFW concentration parameter to be $c_{500} = 3.2$ (Pointecouteau, Arnaud & Pratt 2005; Pratt et al. 2010). The virial radius, r_{vir}, is calculated with spherical collapse model, $r_{vir} = \left[\frac{m_{vir}}{4\pi/3\Delta_c(z)\rho_c(z)}\right]^{1/3}$, where $\Delta_c(z) = 18\pi^2 + 82(\Omega_M(z) - 1) - 39(\Omega_M(z) - 1)^2$ (Bryan & Norman 1998).

Voit et al. (2005) using non-radiative adaptive mesh refinement (AMR) and smooth particle hydrodynamics (SPH) simulations observed that entropy profiles scale as $K_{g,th} \propto r^{1.1-1.2}$ in the range (0.2–1)r_{200} and flatten in the cluster cores. They found differences in the entropy profiles in cluster cores between AMR and SPH. However,

[2]RX J0439.0+0520 and RXC J1023.8-2715 for which the data are not up to $0.3r_{500}$ and Abell 520 for which there is no dominant galaxy that can be considered BCG (Kale et al. 2015a,b) were excluded.
[3]The spectral index, α, for a synchrotron spectrum is defined as $S_\nu \propto \nu^{-\alpha}$, where S_ν is the flux density at frequency ν.
[4]http://szcluster-db.ias.u-psud.fr

Table 1. Basic properties of the clusters sample.

| Cluster	State	z	T_{obs}	M_{500}	L_R 10^{38} keV s^{-1}
–	–	–	keV	10^{14} M$_\odot$	Hz^{-1}
ABELL 0068	NCC	0.25	7.99	6.19	<26.6
ABELL 0141	NCC	0.23	8.90	4.47	9.7 ± 0.3
ABELL 0209	NCC	0.20	8.28	8.17	<16.7
ABELL 0267	NCC	0.22	6.79	4.94	<21.3
ABELL 0521	NCC	0.24	6.74	6.90	2.7 ± 0.4
ABELL 0611	CC	0.28	6.69	5.85	7.8 ± 7.0
ABELL 0697	NCC	0.28	9.06	11.48	11.9 ± 0.5
ABELL 0773	NCC	0.21	8.53	7.08	<18.7
ABELL 0963	CC	0.20	6.60	5.73	49.8 ± 3.3
ABELL 1423	CC	0.21	8.50	6.08	<17.9
ABELL 1576	CC	0.30	8.65	5.98	351.4 ± 7.8
ABELL 1758	NCC	0.27	7.95	7.99	111.0 ± 1.1
ABELL 1763	NCC	0.22	6.90	8.29	7422.7 ± 4.1
ABELL 1835	CC	0.25	7.65	8.46	376.895 ± 5.2
ABELL 2111	NCC	0.22	8.02	5.45	<21.1
ABELL 2163	NCC	0.20	12.12	16.44	<16.1
ABELL 2219	NCC	0.22	9.81	11.00	<20.9
ABELL 2261	CC	0.22	7.58	7.38	66.3 ± 4.0
ABELL 2390	CC	0.23	9.16	9.48	2096.4 ± 4.3
ABELL 2537	CC	0.29	6.08	6.16	<37.8
ABELL 2631	NCC	0.27	9.60	6.96	<32.6
ABELL 2667	CC	0.22	6.31	6.81	187.2 ± 4.1
ABELL 2744	NCC	0.30	9.61	9.55	<40.7
ABELL 2813	NCC	0.29	8.39	9.16	<36.6
ABELL 3088	CC	0.25	6.71	6.70	3.7 ± 0.4
MACS J1115.8+0129	CC	0.34	9.26	6.36	437.8 ± 11.0
MACS J1023.8-2715	NCC	0.30	8.43	8.83	349.1 ± 1.4
MACS J2211.7-0349	CC	0.39	10.51	9.20	<30.5
MACS J2228+2036	NCC	0.41	8.40	7.81	<83.0
MS 1455.0+2232	CC	0.25	4.51	6.20	$<57.5 \pm 5.5$
RX J0439.0+0715	CC	0.24	6.50	5.74	7.9 ± 0.3
RX J1504.1-0248	CC	0.21	8.90	6.97	343.8 ± 3.6
RX J1532.9+3021	CC	0.36	5.44	9.50	372.6 ± 10.6
RX J2129.6+0005	CC	0.23	6.10	4.23	260.8 ± 4.4
ZwCl 0857.9+2107	CC	0.23	12.10	3.10	105.8 ± 4.4
ZWCL 1953	NCC	0.37	14.50	7.39	<63.9
ZWCL 3146	CC	0.28	12.8	5.30	52.7 ± 7.1
ZWICKY 2701	CC	0.21	4.44	4.00	124.1 ± 3.6

Note: Columns (1), (2), (3), (4), (5), and (6) show name, state, redshift, average temperature within the observed radius, m_{500}, and BCG radio luminosity at 1.4 GHz, respectively.

it is now clear that the two results become consistent with one another after accounting for shocks and mixing motions in the SPH case (Mitchell et al. 2009; Vazza et al. 2011). We therefore use the AMR median entropy profile obtained by Voit et al. (2005) and fit it with an appropriate fourth-order polynomial in the whole radial range (Chaudhuri et al. 2013),

$$\frac{K_{g,th}(r)}{K_{200}} = \sum_{i=0}^{4} a_i \left(\frac{r}{r_{200}}\right)^i,$$ (1)

where $K_{200} = 144 \left(\frac{m_{200}}{10^{14} M_\odot}\right)^{2/3} \left(\frac{1}{f_b}\right)^{2/3} h(z)^{-2/3}$ keV cm^2, f_b being the universal baryonic fraction, $h(z) = H(z)/H_0$, and $a_0 = 0.193$, $a_1 = -0.375$, $a_2 = 3.850$, $a_3 = -3.080$, and $a_4 = 0.868$.

The gas density ($n_{g,th}$) and temperature (T_{th}) profiles for theoretical model are obtained by numerically solving hydrostatic equation with an appropriate boundary condition given by $f_g = 0.156$ (Planck Collaboration XIII 2015) at the virial radius (Chaudhuri et al. 2012,
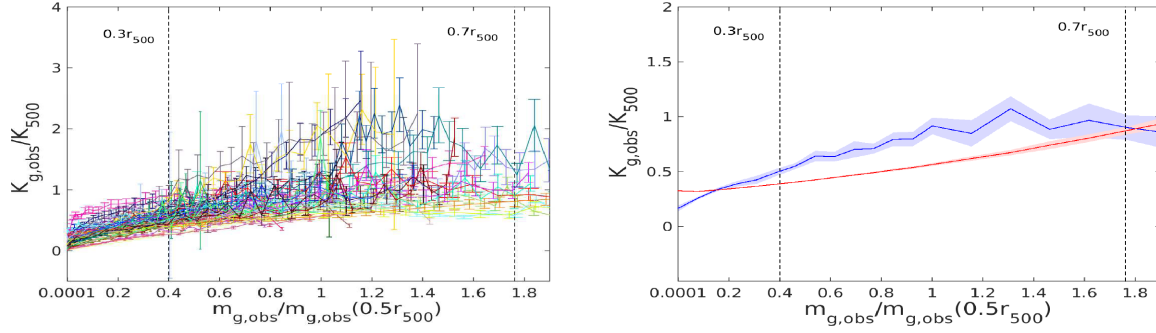
Figure 1. Left-hand panel: observed entropy as a function $m_g/m_g(0.5r_{500})$ for all the clusters. Right-hand panel: comparison of the median observed and theoretical entropy profiles (Voit et al. 2005) as a function $m_g/m_g(0.5r_{500})$. The error bars are at 1σ confidence.
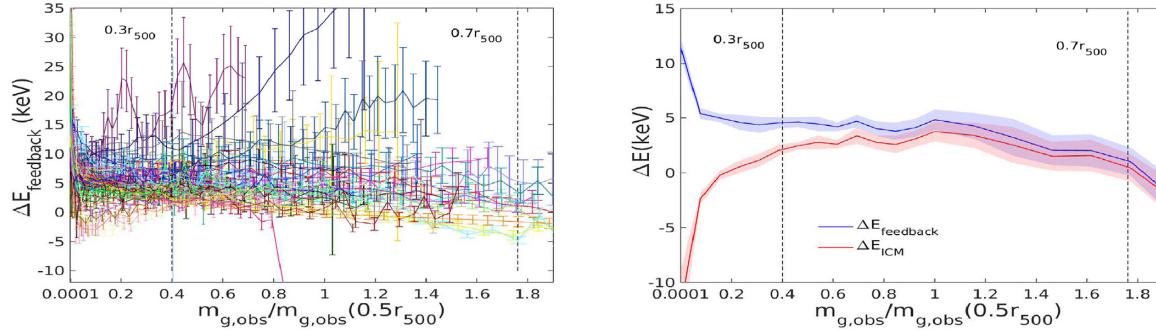
Figure 2. Left-hand panel: non-gravitational energy per particle as a function $m_g/m_g(0.5r_{500})$ for all the clusters. Right-hand panel: comparison of the median of $\Delta E_{\text{feedback}}$ with that of ΔE_{ICM}. The error bars are at 1σ confidence.

2013),

$$\frac{dP_{g,th}(r)}{dr} = -\left[\frac{P_{g,th}(r)}{K_{g,th}(r)}\right]^{3/5} m_p \mu_e^{2/5} \mu^{3/5} \frac{GM(<r)}{r^2}, \quad (2)$$

where $P_{g,th} = n_{g,th} k_B T_{th}$ is the theoretical pressure of ICM and M $(<r)$ is the total mass of cluster within radius r. The left-hand panel in Fig. 1 shows the individual observed cluster entropy profiles as a function of gas mass m_g while the right-hand panel shows the observed median profile and Voit et al. (2005) theoretical median entropy profile for the whole sample. Since entropy is a Lagrangian quantity, we compare the profiles at same gas mass instead of same radii in order to take into account redistribution of gas due to feedback (Nath & Majumdar 2011; Chaudhuri et al. 2012; Iqbal et al. 2017a). At a given mass shell the median profiles were obtained using 1000 bootstrap iterations by means of re-sampling of data points with repetitions. The error bars are then given by root mean square deviation of the distribution. The vertical lines in Fig. 1 approximately define the core region ($r < 0.3r_{500}$) and outside core region ($0.3r_{500} \leq r \leq 0.7r_{500}$). As can be seen there is entropy excess up to $0.7r_{500}$ except at the very centres where the high degree of radiative loss has resulted in the observed entropy being less than theoretical one.

4 ESTIMATES OF FEEDBACK PROFILES

The amount of thermal energy deposition is found to be proportional to $T_{obs}\Delta K/K_{obs}$, where $\Delta K = K_{obs} - K_{th}$. Considering isobaric process, the additional non-gravitational thermal energy per particle in ICM is

$$\Delta Q_{\text{ICM}} = \frac{k_B T_{obs}}{(1 - \frac{1}{\gamma})} \frac{\beta^{2/3}(\beta - 1)}{(\beta^{5/3} - 1)} \frac{\Delta K}{K_{g,obs}}, \quad (3)$$

where $\beta = T_{obs}/T_{th}$. The excess energy per particle is then obtained by adding the change in potential energy in equation (3),

$$\Delta E_{\text{ICM}} = \Delta Q_{\text{ICM}} + G\mu m_p \left(\frac{M_{tot}(r_{th})}{r_{th}} - \frac{M_{tot}(r_{obs})}{r_{obs}}\right), \quad (4)$$

where r_{th} and r_{obs} are theoretical and observed radii, respectively, enclosing the same gas mass.

Finally, the total feedback energy/particle can be found after adding the energy lost due to radiative cooling,

$$\Delta E_{\text{feedback}} = \Delta E_{\text{ICM}} + \Delta L_X t_{age}, \quad (5)$$

where ΔL_X is the bolometric luminosity emitted by the ICM in a given shell which is estimated by averaging theoretical and observed cooling functions, Λ_N of Tozzi & Norman (2001). t_{age} is the age of the shell which is calculated using the expression of mass acceration rate given by Voit et al. (2003) for clusters of present-day mass $\approx 10^{15}$ M$_\odot$ and taking the age of Universe to be 13.47 Gyr. The total excess energy deposited within the radius r is given by $E_{\text{feedback}} = \frac{1}{\mu_g m_p} \int_0^r \Delta E_{\text{feedback}} \, dm_g$, where $\mu_g = 0.6$ is the mean molecular weight of gas and m_p is mass of proton. The average energy/particle ($\epsilon_{\text{feedback}}$) is found by dividing E_{feedback} with the total number of gas particles $N(r)$.

In Fig. 2, the left-hand panel shows the non-gravitational energy profiles as a function of gas mass m_g for individual clusters and the right-hand panel shows the median non-gravitational feedback energy with and without adding energy lost due to cooling. At par with earlier findings of Chaudhuri et al. (2012) and Iqbal et al. (2017a), our results also find significant entropy and hence evidence of feedback energy in the cluster inner regions. Moreover, as can be seen the radiative loss is only important up to $0.3r_{500}$. We find that the average feedback energy per particle $\epsilon_{\text{feedback}}$ to be 4.32 ± 0.52 keV

Table 2. Best-fitting scaling relations and Spearman's rank correlation coefficient (r).

Method	A	B	r	A	B	r
		Full sample			Radio detection only	
		$\log(E_{\text{feedback}}/10^{70}\,\text{keV}) = A + B\log(T/8\,\text{keV})$				
EM	1.06 ± 0.05	1.56 ± 0.47	0.52	–	–	–
Bayesian	1.12 ± 0.05	0.98 ± 0.37	–	–	–	–
		$\log(L_R/10^{38}\,\text{keV s}^{-1}\,\text{Hz}^{-1}) = A + B\log(m_{g,\text{obs}}/10^{13}\,\text{M}_\odot)$				
EM	1.31 ± 0.19	1.17 ± 0.71	0.31	1.76 ± 0.16	1.78 ± 0.61	0.57
Bayesian	1.60 ± 0.13	1.22 ± 0.53	–	1.76 ± 0.19	1.76 ± 0.71	–
		$\log(L_R/10^{38}\,\text{keV s}^{-1}\,\text{Hz}^{-1}) = A + B\log(L_{X,\text{obs}}/10^{53}\,\text{M}_\odot)$				
EM	0.81 ± 0.31	0.91 ± 0.35	0.42	1.25 ± 0.27	0.95 ± 0.30	0.60
Bayesian	1.17 ± 0.23	0.81 ± 0.27	–	1.27 ± 0.32	0.94 ± 0.35	–
		$\log(L_R/10^{38}\,\text{keV s}^{-1}\,\text{Hz}^{-1}) = A + B\log(M_{\text{vir}}/10^{14}\,\text{M}_\odot)$				
EM	2.11 ± 1.38	-0.64 ± 1.32	0.02	0.50 ± 1.36	1.43 ± 1.32	0.38
Bayesian	1.53 ± 1.00	0.23 ± 0.94	–	0.53 ± 1.57	1.41 ± 1.53	–

Note: E_{feedback}, $L_{X,\text{obs}}$, and $m_{g,\text{obs}}$ are estimated within $0.3r_{500}$.
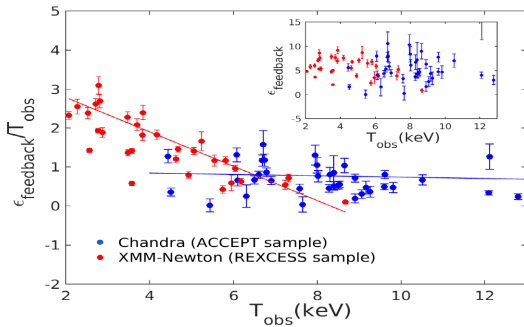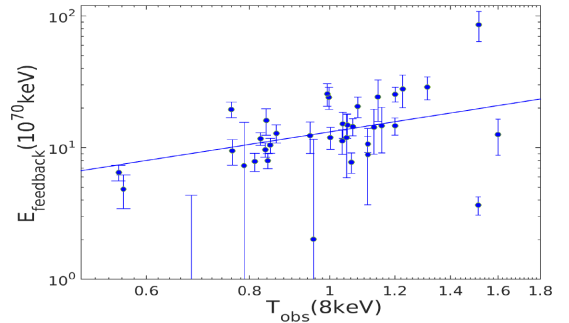

Figure 3. Comparison of $\epsilon_{\text{feedback}}/T_{\text{obs}}$ between REXCESS sample (Pratt et al. 2010) and our *Chandra* sample of high-temperature clusters (>6 keV). Solid blue and red lines show the best fit for *Chandra* and REXCESS samples, respectively. The inset shows the feedback energy per particle.

Figure 4. Correlation between E_{feedback} and T_{obs}. Solid blue line represents Bayesian best fit.

in the region $(0.01–0.3)r_{500}$ and 4.54 ± 0.55 keV in the region $(0.01–0.5)r_{500}$.

Fig. 3 shows the ratio of the non-gravitational feedback energy over energy from gravitational collapse, $\epsilon_{\text{feedback}}/T_{\text{obs}}$ as a function of T_{obs} in the region $(0.01–0.3)r_{500}$ for our sample and for REXCESS sample.[5] It can be clearly seen that there is a higher degree of feedback for the REXCESS sample which are mainly low-temperature clusters (<6 keV) compared to our sample which are high-temperature clusters (>6 keV). This shows that for low-temperature (mass) clusters, the AGN feedback is more effective in transferring energy into ICM. A simple linear fitting of $\epsilon_{\text{feedback}}/T_{\text{obs}}$ $= b_1 T_{\text{obs}} + b_0$ yields $b_1 = -0.01 \pm 0.03$, $b_0 = 0.915 \pm 0.30$ for our sample and $b_1 = -0.44 \pm 0.05$, $b_0 = 3.66 \pm 0.23$ for REXCESS sample. Our result corroborates previous works on the non-gravitational feedback (McNamara & Nulsen 2007; Fabian 2012).

5 CORRELATIONS OF THE FEEDBACK ENERGY AND BCG RADIO LUMINOSITY

Since the effect of AGN feedback is dominant only in the cluster inner regions (Gaspari et al. 2014; Iqbal et al. 2017a), we correlate clusters quantities measured within $r = 0.3r_{500}$ (except for temperature) in order to gain a meaningful picture of AGN–ICM interaction. To estimate correlations we fit the power-law relations

using linear regression in log–log space. The regression is first performed using parametric EM (Expectation Maximization) algorithm that is implemented in the ASURV package (Isobe, Feigelson & Nelson 1986). Since ASURV does not take errors into account, we also consider Bayesian regression algorithm implemented in LINMIX package[6] (Kelly 2007) which takes heteroscedastic and intrinsic scatter into account. However, both the algorithms incorporate upper limits. We quote results from Linmix although both packages give similar results. To study the correlations of the BCG radio luminosity, we consider full sample as well as sub-sample of radio detected BCG clusters. Since detection sample is dominated by CC clusters and non-detection sample is dominated by the NCC clusters, it makes sense in separating the sample in these two groups. Table 2 gives the best-fitting results and correlation coefficient between various cluster parameters. In general, we find that for the radio detected sample, the best-fitting lines have steeper slopes with larger values of correlation coefficient compared to those from the full sample.

Fig. 4 shows the correlation between E_{feedback} and T_{obs}. We find $E_{\text{feedback}} \propto T_{\text{obs}}^{0.98 \pm 0.37}$ with a correlation coefficient of 0.52 for the full sample. This suggests that for massive clusters (high temperature), although, as discussed in the previous section the fraction increase in energy per particle is small, the total feedback energy is large. Further, higher total mass also implies higher gas mass (or N) which makes feedback energy per particle ($\epsilon_{\text{feedback}}$) more or less constant for all temperature range (see the inset in Fig. 3). From the

---

[5]We recalculated the values in Chaudhuri et al. (2013) for REXCESS sample including our equation (5).
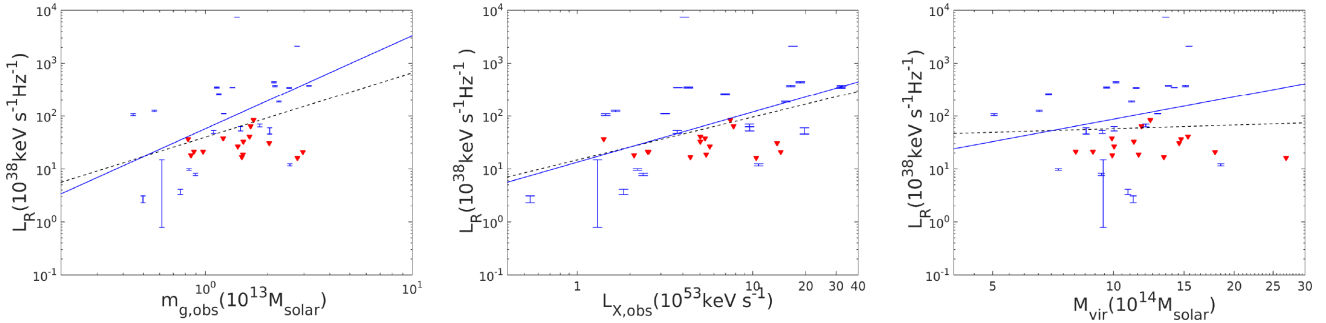
Figure 5. Left-hand panel: correlation between L_R and $m_{g,\,obs}$. Middle panel: correlation between L_R and $L_{X,\,obs}$. Right-hand panel: correlation between L_R and M_{vir}. Solid blue and dashed black lines represent Bayesian best fit for the full sample and sub-sample (BCG detected), respectively. Blue and red markers represent radio detection and radio non-detection samples, respectively.

self-similar consideration ($N \propto m_{g,obs} \propto M_{tot} \propto T_{obs}^{3/2}$), one obtains $\epsilon_{feedback} = E_{feedback}/N \propto T_{obs}^{0.5\pm0.37}$ which roughly agrees at 1σ level with our results.

The left-hand panel of Fig. 5 shows the correlation between L_R and $m_{g,\,obs}$. We find the scalings $L_R \propto m_{g,obs}^{1.22\pm0.53}$ with the correlation coefficient of 0.31 for full sample and $L_R \propto m_{g,obs}^{1.76\pm0.71}$ with the correlation coefficient of 0.57 for sub-sample. The middle panel of Fig. 5 shows the correlation of L_R with $L_{X,\,obs}$. We find $L_R \propto L_{X,obs}^{0.81\pm0.27}$ with the correlation coefficient of 0.42 for the full sample and $L_R \propto L_{X,obs}^{0.94\pm0.35}$ with the correlation coefficient of 0.60 for sub-sample. This confirms the fact that radio luminosity is proportional to the mass accretion rate which in turn depends on the gas mass and hence X-ray luminosity.

Finally, the right-hand panel of Fig. 5, shows the correlation between the L_R and M_{vir} for which we obtain the poor estimates of the fitted parameter and weak correlation coefficient. We find $L_R \propto M_{vir}^{0.23\pm0.94}$ with the correlation coefficient of 0.02 for the full sample and $L_R \propto M_{vir}^{1.41\pm1.53}$ with the correlation coefficient of 0.38 for the sub-sample.

6 DISCUSSION AND CONCLUSIONS

Our finding of the above scaling between BCG radio luminosity L_R and the cluster virial mass has important implications. It is also consistent with previously discovered scalings, as we will discuss below.

Franceschini, Vercellone & Fabian (1998) found that black hole mass (M_{BH}) in AGNs scales with radio luminosity as $L_R \propto M_{BH}^{2.5}$. There is also a relation between the total mass of a massive elliptical galaxy (M_{BCG}), $M_{BH} \propto M_{BCG}^{1.4}$ (Reines & Volonteri 2015). Moreover, SDSS studies such as Behroozi, Conroy & Wechsler (2010) show that for such massive galaxies, the stellar mass $M_{*,\,BCG}$ scales as $M_{BCG}^{0.3}$. Combining these three scalings together, we find that $L_R \propto M_{*,BCG}^{2.5\times1.4/0.3} = M_{*,BCG}^{11.7}$. In addition, $M_{*,\,BCG}$ scales with M_{vir} of the parent cluster with a slope 0.12 ± 0.03 (Whiley et al. 2008). Using this, we obtain $L_R \propto M_{vir}^{1.4}$ which is consistent with our results for the sub-sample of radio detected BCG clusters.[7] Further combining $L_R \propto M_{BH}^{2.5}$ with our results of $L_R \propto M_{vir}^{1.29\pm1.59}$, one finds $M_{BH} \propto M_{vir}^\beta$, with $\beta = 0.56_{-0.60}^{+0.61}$ for the sub-sample which is consistent with Roychowdhury et al. (2005), who found $M_{BH} \propto M_{vir}^1$ from excess entropy consideration.

Our finding that the feedback energy for a given radio luminosity decreases with increasing cluster mass (or temperature) also deserves attention. If the energy deposited by the radio source is through the dynamics of the cocoon, then one expects a constant fraction of the total energy of the radio source to be given as feedback energy, e.g. as derived by Bicknell, Dopita & O'Dea (1998; their equation 2.13). Clearly, this is not tenable in light of our finding. However, it has been previously discussed in the literature that the efficiency of energy deposition may be larger for low-mass clusters. Fabian (2012) has suggested that weak shocks (expected in hot ICM of massive clusters) are poor at dissipating energy, and McNamara & Nulsen (2007) suggested that a lower binding energy per particle in groups may lead to a greater efficiency of non-gravitational heating in low-mass clusters. The high probability of radio detections in CC clusters suggests that it depends on the dynamical state of host cluster. Nevertheless, mergers may transform CC clusters into NCC clusters with enhanced ICM entropies. Alternatively, the lack of radio emission in the NCC clusters to account for the excess entropy suggests that clusters were pre-heated before cluster formation (Dwarakanath & Nath 2006).

Since L_R is directly linked with the thermal properties of the ICM, this motivates us to look for a relation between $E_{feedback}$ and L_R. For the current sample, we did not find any significant correlation between $E_{feedback}$ and L_R, probably because $E_{feedback}$ is the integrated quantity and L_R is the current property. However, some possibility of separating the sample into the clusters where the radio emission is very recent (and hence not much energy has been injected into ICM) and clusters where radio feedback has happened in the distinct past, one might be able to find interesting clues about $E_{feedback}-L_R$ relation and would be an interesting extension of the work.

In summary, our study suggests that the non-thermal emission from the BCGs is directly linked with the feedback energy and the thermodynamic properties of the ICM. We find moderate correlation of the feedback energy and BCG radio luminosity with the cluster properties. Our results suggest clusters which are radio detected and those without correlate differently with the ICM properties. Studies such as ours can be a powerful tool to study the connection between BCGs (which are mostly found in CC clusters) and ICM thermodynamics and understanding dynamical/evolutionary differences of CC clusters from their NCC counterparts. Lastly, with the upcoming and future radio data such as from SKA, it will be possible to obtain much tighter constraints on the scaling relations to better understand the effects of feedback on the cluster properties.

---

[7]If one instead uses a slope of 0.42 ± 0.07 (Chiu et al. 2016; their fig. 2) for $M_{*,\,BCG} - M_{vir}$ relation, then this gives $L_R \propto M_{vir}^{4.9}$.

REFERENCES

Bartelmann M., Schneider P., 2001, Phys. Rep., 340, 291
Behroozi P. S., Conroy C., Wechsler R. H., 2010, ApJ, 717, 379
Bicknell G. V., Dopita M. A., O'Dea C. P. O., 1998, ApJ, 485, 112
Bryan G. L., Norman M. L., 1998, ApJ, 495, 80
Cassano R., Ettori S., Giacintucci S., Brunetti G., Markevitch M., Venturi T., Gitti M., 2010, ApJ, 721, L82
Cavagnolo K. W., Donahue M., Voit G. M., Sun M., 2009, ApJS, 182, 12
Chaudhuri A., Nath B. B., Majumdar S., 2012, ApJ, 759, 5
Chaudhuri A., Majumdar S., Nath B. B., 2013, ApJ, 776, 84
Chiu I. et al., 2016, MNRAS, 455, 258
Condon J. J., Cotton W. D., Greisen E. W., Yin Q. F., Perley R. A., Taylor G. B., Broderick J. J., 1998, AJ, 115, 1693
Dwarakanath K. S., Nath B. B., 2006, ApJ, 653, L9
Eckert D., Molendi S., Vazza F., Ettori S., Paltani S., 2013, A&A, 551, A22
Fabian A. C., 2012, ARA&A, 50, 455
Franceschini A., Vercellone S., Fabian A. C., 1998, MNRAS, 297, 817
Gömöry P., Beck C., Balthasar H., Rybák J., Kučera A., Koza J., Wöhl H., 2010, A&A, 511, 14
Gaspari M., Brighenti F., Temi P., Ettori S., 2014, ApJ, 783, L10
Gladders M. D., Yee H. K. C., Majumdar S., Barrientos L. F., Hoekstra H., Hall P. B., Infante L., 2007, ApJ, 655, 128
Iqbal A., Majumdar S., Nath B. B., Ettori S., Eckert D., Malik M. A., 2017a, MNRAS, 465, L99
Iqbal A., Majumdar S., Nath B. B., Ettori S., Eckert D., Malik M. A., 2017b, MNRAS, 472, 713
Isobe T., Feigelson E. D., Nelson P. I., 1986, ApJ, 306, 490
Kale R., Venturi T., Cassano R., Giacintucci S., Bardelli S., Dallacasa D., Zucca E., 2015a, A&A, 579, 92
Kale R., Venturi T., Cassano R., Giacintucci S., Bardelli S., Dallacasa D., Zucca E., 2015b, A&A, 581, 23
Kelly B. C., 2007, ApJ, 665, L1489
Mantz A., Allen S. W., Ebeling H., Rapetti D., Drlica-Wagner A., 2010, MNRAS, 406, 1773
McNamara B. R., Nulsen P. E. J., 2007, ARA&A, 45, 117
Mitchell N. L., McCarthy I. G., Bower R. G., Theuns T., Crain R. A., 2009, MNRAS, 395, 180
Nath B. B., Majumdar S., 2011, MNRAS, 416, 271
Nath B. B., Roychowdhury S., 2002, MNRAS, 333, 145
Navarro J. F., Frenk C. S. W, S. D. M., 1996, ApJ, 462, 563
Planck Collaboration V, 2013, A&A, 571, A29
Planck Collaboration XIII, 2015, A&A, 594, A20
Pointecouteau E., Arnaud M., Pratt G. W., 2005, A&A, 435, 1
Reines A. E., Volonteri M., 2015, ApJ, 813, 82
Roychowdhury S., Ruszkowski M., Nath B. B., 2005, ApJ, 634, 90
Tozzi P., Norman C., 2001, ApJ, 546, 63
Vazza F., Dolag K., Ryu D., Brunetti G., Gheller C., Kang H., Pfrommer C., 2011, MNRAS, 418, 960
Venturi T., Giacintucci S., Dallacasa D., Cassano R., Brunetti G., Bardelli S., Setti G., 2008, A&A, 484, 327
Voit G. M., Balogh M. L., Bower R. G., Lacey C. G., Bryan G. L., 2003, ApJ, 593, 272
Voit G. M., Kay S. T., Bryan G. L., 2005, ApJ, 364, 909
Whiley I. M. et al., 2008, MNRAS, 387, 1253

This paper has been typeset from a TEX/LATEX file prepared by the author.